An Analysis of the Risk from UAS Missions in the National Airspace

Armand Awad

A thesis submitted in partial fulfillment of the requirements for the degree of

Master of Science in Aeronautics & Astronautics

University of Washington

2013

Committee

Juris Vagners, Chair

Kristi Morgansen

Christopher Lum

Program Authorized to Offer Degree:
Department of Aeronautics & Astronautics

University of Washington

Abstract

An Analysis of the Risk from UAS Missions in the National Airspace

Armand Awad

Chair of the Supervisory Committee:
Professor Emeritus Juris Vagners
Department of Aeronautics & Astronautics

As Unmanned Aerial Systems (UAS) are integrated into the national airspace, we must be careful to ensure that the hazard rate to human bystanders is sufficiently small. The first source of risk to bystanders involves midair collisions between UAS and other aircraft. The second source of risk concerns risks due to ground impact, both the bystander hazard rate due to aircraft impacting the ground as well as the dependence of crash rate on location. Here, we present first-order models adapted from the literature which estimate the risk due to these various scenarios. Model verification is then achieved through extensive analysis of historic civil aviation accidents. From this, we gain two major insights. First of all, we show that UAS already achieve manned levels of safety with respect to midair collisions. This is because general aviation aircraft routinely operate in conditions where see-and-avoid is used but is not effective. Secondly, we find that the risk due to ground collision of UAS is sufficiently small to allow operations over the majority of the United States. The models presented here are powerful tools that can be used by a general audience to objectively assess the risks associated with various missions in the national airspace.

TABLE OF CONTENTS

LIST OF FIGURES

GLOSSARY

C_{RANDOM}, C_{ACTUAL}: Random particle and actual midair collision rates, respectively

N_I: Number of planes of species i

A_{AB}: Effective collision cross section

D_I: Characteristic dimension of species i

U_I: Velocity of species i

V_{AB}: Volume over which species roam

F: Control influence factor

σ_P, $\sigma_{POPULATION}$: Pedestrian and population densities, respectively

W_{UA}, L_{UA}: UAV wingspan and length, respectively

γ: UAV flide angle

R_P, H_P: Characteristic pedestrian radius and height, respectively

λ: Average aircraft crash frequency

I_{CRASH}, $I_{FLIGHT\,HOUR}$: Expected injuries per crash and per flight hour, respectively

$P(R)$: Crashes per movement as a function of distance from airport

$I_{AIRPORT\,PER\,MOVEMENT}$: Injuries per movement near airport as a function of distance

$I_{CUM.\,PER\,MOVEMENT}$: Cumulative injuries per movement near airport as a function of distance

$I_{DENSITY\,PER\,MOVEMENT}$: Injury density per movement near an airport

$I_{CUM.\,DENSITY\,PER\,MOVEMENT}$: Cumulative injury density per movement near an airport

$I_{BYSTANDER\,PER\,MOVEMENT}$: Bystander perspective injuries per movement near an airport

$I_{CUM.\,BYSTANDER\,PER\,MOVEMENT}$: Cumulative bystander perspective injuries per movement near an airport

ACKNOWLEDGMENTS

The author wishes to express sincere appreciation to his fellow graduate students in the AFSL as well as the NDCL, and in particular to his advisor Juris Vagners.

Chapter 1

INTRODUCTION

Unmanned Aerial Systems (UAS) have existed in one form or another since the early twentieth century. In the past decade, this technology has matured enough to come into widespread use. And, while adoption of UAS has been primarily among the military, many civilian applications have also been proposed. For example, UAS could be used to monitor remote pipelines or search for lost hikers in the woods, in environments where the use manned aircraft is either not economically or physically feasible. Until recently, the rules concerning civilian operation of UAS in the United States have been either unclear or very prohibitive. However, the advent of the FAA Modernization and Reform Act of 2012 [2] is expected to change this, with regulations being put in place that will aid the integration of UAS into the national airspace.

While there are many concerns about UAS being operated in civilian airspace, paramount among these considerations is the inherent risk of flying missions in the national airspace. In particular, the risk to human bystanders must be acceptably low. In this, risk for UAS differs from manned aircraft. In the latter case, the focus must be on high reliability; any failure endangers the human pilot as well as any passengers within. For UAS, on the other hand, higher failure rates may be acceptable as long as no bystanders are harmed. For example, the crash of a UAS in an empty field may result in monetary losses from repairs to the aircraft as well as reparations to the field's owner for any property damage, but not in loss or injury to human lives. There are therefore two main sources of risk from UAS missions in the national airspace [3, 4]. The first is the threat of midair collisions between UAS and other aircraft. The second is the hazard to surface-level bystanders from ground collisions of UAS.

Historically, midair collisions have been viewed as the primary safety issue by the public [5]. As a result, the FAA has advised that UAS achieve an "equivalent level of safety" to manned aircraft. A lot of the research in this field has been focused on creating models for aircraft encounters from a Bayesian standpoint [6], some even modeling the effects of aircraft traffic lanes [7]. Work has also focused on creating and analyzing collision avoidance systems, both in managed [8] and unmanaged [9] airspace. However, by analyzing historical manned midair collisions we will show that not only are midair collisions not the primary source of risk to bystanders, but that UAS already achieve manned levels of safety in this domain.

With respect to the risk from ground collisions, once again a lot of work has been focused on modeling injuries and fatalities to bystanders. This has been donebased on kinetic energy considerations [10] as well as based on a "gliding impact" model [1, 11, 12], which is our focus here. While simple analysis has been performed in many of these cases, we present a detailed and in depth verification of the model including the impact of various parameters on the hazard rate. Previous research has also looked into modeling the distribution of aircraft impact locations [13] as well as how crash rates vary near airports and risk from the perspective of bystanders [14]. In the following, we extend this work by focusing on how location-dependent failure rates have historically affected safety for bystanders near airports.

In Section 2, we discuss the methodology used for gathering and processing the historical data used throughout this paper. Section 3 analyzes the risk of midair collisions, while Section 4 does the same for ground collisions. Finally, Section 5 presents examples of UAS mission risk analysis, both from a broad perspective and from a detail-oriented one.

Chapter 2

DATA AND PROCESSING METHODOLOGY

2.1 Data Sources

In this thesis, historical data from manned aviation accidents are used to evaluate and investigate models of the hazard presented to bystanders by UAS. These data were primarily gathered from the National Transportation Safety Board (NTSB) [15], which investigates and subsequently publishes data on all civil aviation accidents in the United States. For every accident/incident, this includes the city and state, aircraft make and model, and number of people seriously injured or killed on the ground in each event. Further data was gathered from the US Census Bureau [16] on the population and land area of each event city, and from various sources including the manufacturers when possible, on the wingspan of each aircraft involved in an event. The distance from the airport was also measured using incident report descriptions [17, 18] for accidents located near several major airports. Finally, civil aviation statistics were compiled from FAA publications [19].

2.2 Processing and Analysis

For ground collisions, further processing of the accident data is necessary. Two key factors were calculated. The first was population density, computed using US Census data for the site of the event. This is important in ground collisions as the more dense a population a crash occurs in, the more people are likely to be hurt by the impact itself as well as by any subsequent damage (such as fires, structural damage, etc). The second item was scaled ground injuries, which was calculated using the reported bystander injuries and scaling using the wingspan of the aircraft. Since

larger aircraft will cause a greater impact area and thus more injuries than a smaller aircraft, this factor was devised in order to be able to compare injuries between potentially very different sizes of aircraft (say, when seeing how injuries scale with population density). This impact area is related to both the length and the wingspan of the aircraft, but since aircraft length scales roughly linearly with wingspan, we use wingspan as a simplified scaling factor here. Thus, for two accidents involving differently-sized aircraft, both sets of bystander injuries would be scaled to that of a given wingspan aircraft before comparison using each accident's respective wingspan and the bystander injuries per crash model, discussed discussed in Section 4.1.

There are several ways of visualizing the processed accident data. The first uses a histogram to plot population density bins versus average scaled ground injuries in each bin, and can be seen in figure 2.1. This binning and averaging was performed in order to derive a measure of the predicted number of injuries given an accident in a certain size city. A second method expands on the histogram idea, and instead uses a "moving bin" to help eliminate sensitivity to bin location. The injuries at each population point p for this floating histogram are then calculated as

$$\text{Injuries}(p) = \text{mean}\left(\left\{\text{Scaled Injuries}(k)\middle| p-\delta < k \leq p+\delta\right\}\right)$$

An example of such a floating histogram is shown in figure 2.2, where average historical injuries are plotted against aircraft wingspan. We can see that these two agree well, with the floating histogram providing more finely-grained data. For these reasons, the floating histogram is the preferred visualization method, and is used throughout the thesis.

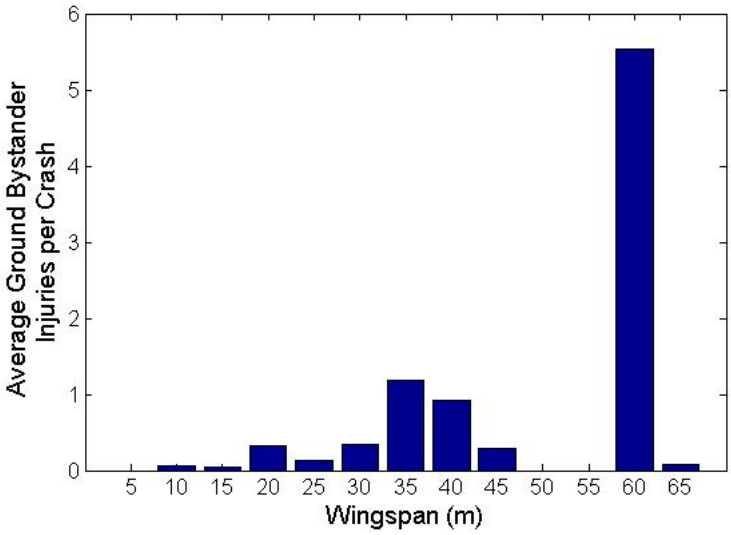

Figure 2.1: Histogram of Historical Ground Hazard Rate versus Aircraft Wingspan

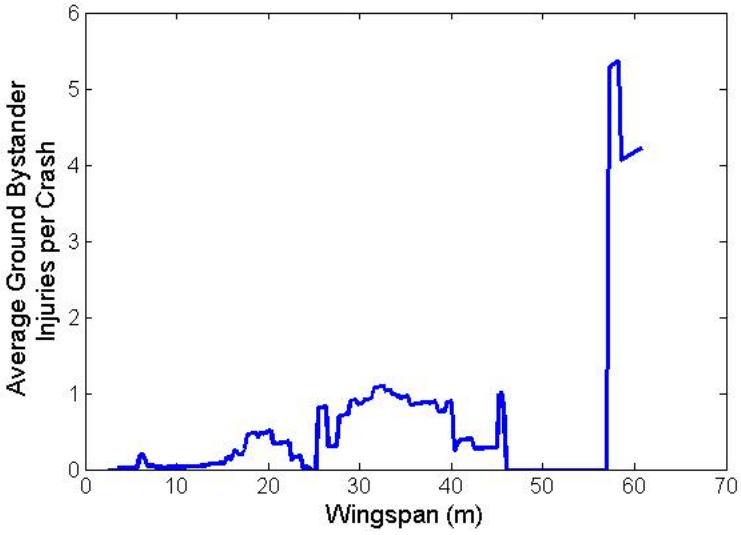

Figure 2.2: Floating Histogram of Historical Ground Hazard Rate versus Aircraft Wingspan

Chapter 3
MIDAIR COLLISION RISK

One important source of human safety hazard from UAS is the risk of midair collisions. The importance of this source is twofold, as it includes both the direct risk of UAS colliding with manned aircraft as well as the indirect hazard caused by an increase in ground collisions from UAS colliding with either manned or unmanned aircraft. Since UAS must reach "equivalent manned levels" of safety for successful integration into the national airspace, a method of quantifying the historical midair collision hazard is necessary. Following the work of Anno [20], we use the random particle collision model as a normalizing factor to compute a "control influence factor" which can be used as a measure of safety for midair collisions.

3.1 Random Particle Collision Model and the Control Influence Factor

Consider a large number of aircraft flying in a particular airspace. If no effort is made to avoid collisions between the aircraft, then we expect that a fixed collision rate, C_{Random}, will exist between them. This collision rate will depend on how many aircraft are roaming at any given time, their characteristic sizes and speed, and the volume over which they roam. This is the basis of the random particle collision model, which can also be used to model the collision rates of, for example, gaseous molecules propagating in a fixed volume.

For aircraft species A and B, the random particle collision model predicts a collision rate

$$C_{Random} = \frac{N_A N_B}{\sigma} a_{AB} \frac{u_{AB}}{V_{AB}} \tag{3.1}$$

where N_i is the average number of planes of species i in the air, a_{AB} is the effective collision cross section given by

$$a_{AB} = \frac{\pi}{4}(D_A + D_B)^2 \tag{3.2}$$

where D_i is a characteristic dimension

$$D_i = \frac{\text{length} + \text{width} + \text{height}}{3} \tag{3.3}$$

, u_{AB} is the average velocity between the planes given by

$$u_{AB} = \frac{1}{2}(u_A + u_B) \tag{3.4}$$

, V_{AB} is the volume over which the plane species fly, and σ is a symmetry factor that is 1 when species A is not like species B and 2 for similar species of aircraft.

Now, using the random collision rate as a normalizing component, we define the control influence factor, F, as

$$F \equiv \frac{C_{Random}}{C_{Actual}} \tag{3.5}$$

As the name implies, this factor can be used to quantify the influence of collision mitigation techniques (*e.g.*, see-and-avoid or sense-and-avoid), and therefore the safety level. If F is greater than one, then a given technique is positively affecting safety from the no avoidance case (higher is better). However, if F is less than one, then safety between aircraft is somehow being impeded.

3.2 Historical Manned Midair Collisions

In order to provide a baseline for the risk due to UAS midair collisions, we must look at what has been historically acceptable for manned aircraft. Figure 3.1 presents the historic number of manned collisions in the United States from 1974 through 2008, classified as either between two general aviation aircraft, between two air carrier aircraft, or between a general aviation aircraft and an air carrier aircraft. We can see that few collisions have historically occurred between air carrier aircraft or between

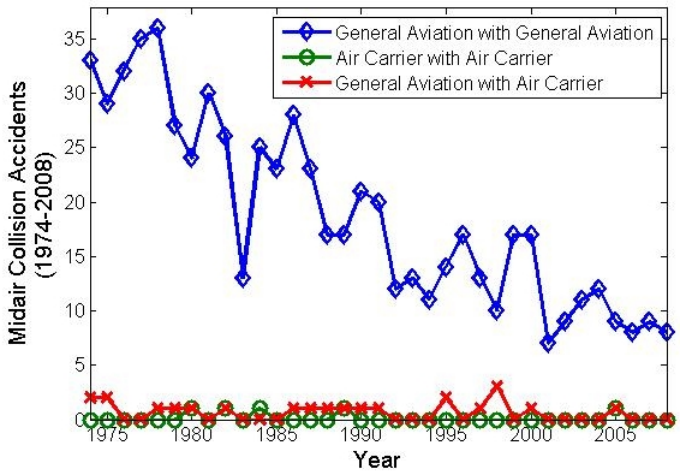

Figure 3.1: Historic Midair Collisions (1974–2008)

an air carrier aircraft and a general aviation aircraft, while a significant number of collisions have occurred between general aviation aircraft.

In order to evaluate the historic safety levels between these aircraft classifications, the human-control influence factor is calculated. Following Anno [20], we represent general aviation aircraft by the Cessna Model 150 and air carrier aircraft by the Boeing Model 747; relevant data for these aircraft are shown in Table 3.1. The resulting comparison of the safety levels between these collision classifications is shown in Table 3.2. As we might expect, the meticulously overseen air carriers have a very high human-control influence factor of 3261, indicating a high level of safety. This is also true of interactions between air carrier and general aviation aircraft, with a influence factor of 1466. However, we see that the overall interaction among general aviation aircraft is much less safe, with a human-control influence factor of only 1.54. Due to the preponderance of data in this category, and since we are interested in the minimum safety level that manned aircraft achieve, further investigations in the category of general aviation aircraft collisions are merited.

By examining the historical, general aviation, midair collision data, we find that

	General Aviation Cessna Model 150	Air Carrier Boeing Model 747
Wingspan	33-ft 2-in	195-ft 8-in
Length	23-ft 8-in	231-ft 10-in
Height	9-ft 7-in	63-ft 5-in
Ave. Cruising Speed	117 mph	450 mph
Service Ceiling	14,000 ft	39,000 ft

Table 3.1: Characteristic Aircraft Data

Type of Collision	Predicted Rate (collisions/yr)	Historical Rate (ave. collisions/yr)	F_{Human}
$\left(\frac{\text{General Aviation}}{\text{General Aviation}}\right)$	29.8	19.3	1.54
$\left(\frac{\text{General Aviation}}{\text{Air Carrier}}\right)$	879.7	0.6	1466
$\left(\frac{\text{Air Carrier}}{\text{Air Carrier}}\right)$	326.1	0.1	3261

Table 3.2: Comparison of Random Collision Theory with Historical Data (1974–2008)

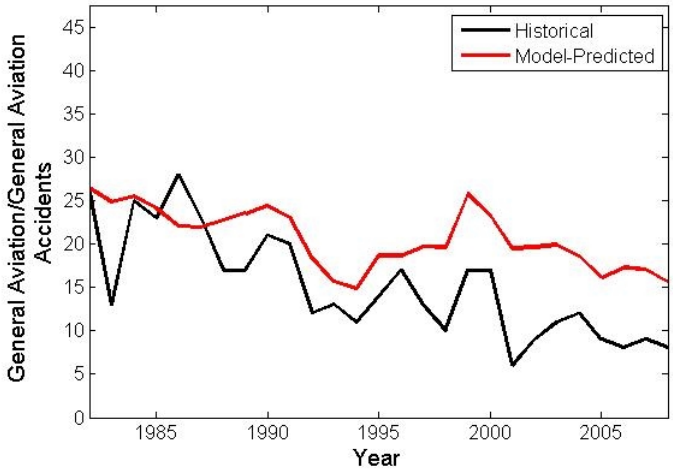

Figure 3.2: U.S. General Aviation Midair Collisions under VMC (1982–2008)

the vast majority of collisions occur under visual meteorological conditions (VMC). Figure 3.2 therefore compares the progression between 1982 and 2008 of historical midair collisions under VMC to the random particle model using general aviation VMC hours flown per year. We can see that the random particle model matches the historic data fairly closely, usually over-predicting the number of collisions per year. This indicates a human-control influence factor of just above unity, similar to that found with the overall general aviation data. However, if we further subdivide the collisions between those occurring during the day and those that occurred at night, the picture becomes much more interesting. Table 3.3 presents these results, using general aviation VMC day hours flown and night hours flown publicly available from the FAA for the random particle model inputs. In the case of general aviation aircraft operating at night under VMC, we see that *more* collisions occurred historically than was predicted by the random particle model, resulting in a human-control influence factor of only 0.90.

Two major conclusions can be drawn from this result. First of all, it is clear that general aviation aircraft do not statistically avoid collisions under these circum-

Condition	Actual Collisions	Predicted Random Collisions	F_{Human}
VMC	407	559.3	1.37
VMC Day	394	432.8	1.09
VMC Night	9	8.1	0.90

Table 3.3: Cumulative U.S. General Aviation Midair Collisions (1982–2008)

stances. Since pilots generally fly under visual flight rules in these conditions, this lack of mitigation indicates a failure of the see-and-avoid policy at night. Secondly, this result implies that UAS *already* achieve manned levels of safety with respect to midair collision rates. While implementations of sense-and-avoid systems will only improve UAS safety levels, they are not necessary to meet the minimum requirement of "equivalent manned levels" in the first place.

Chapter 4
GROUND COLLISION RISK

For surface-level bystanders, the hazard from UAS comes from ground impact of the aircraft. There are three issues of interest here. The first is the bystanders injury rate per crash. How many bystanders on the ground will get injured if a crash occurs in a given location? The second is the issue of how likely a crash is. How often and under what conditions do crashes occur? Finally, the third issue involves the risk from a bystander's perspective. How likely is it that an individual, surface-level bystander will be harmed by a UAS mission? Beginning with a simple ground injury model from Lum and Waggoner [1], we use historic manned aircraft accident data from the NTSB to verify the model and to investigate these questions.

4.1 Bystander Injuries per Crash Model

4.1.1 Aircraft Crash Hazard

In order to estimate the overall risk due to ground collision over a proposed UAS mission, we desire a simple method of accounting for the injuries to bystanders given that an aircraft crash occurs in a given location. Intuition tells us that the number of injuries that occur per crash should be related to the characteristics of the aircraft (particularly aircraft size and glide ratio) as well as the population density where the crash occurs. For instance, a large aircraft will likely injure more bystanders than a small two-seater during a crash if all other factors are equal.

Here, we use a "gliding crash" model of ground collision as presented by Lum and Waggoner [1]. In this model, it is assumed that bystander population is on average evenly distributed and that the aircraft glides to the ground at an angle γ. When

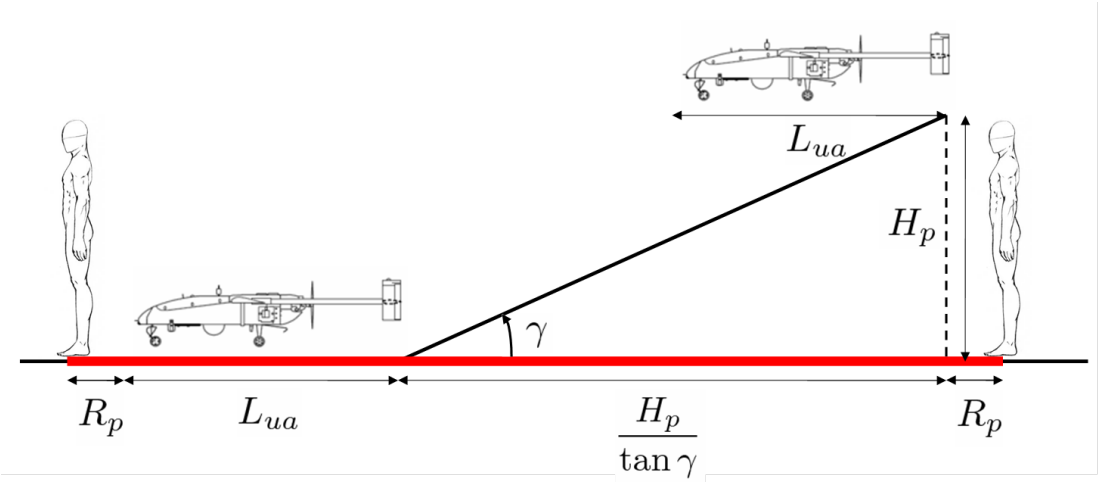

Figure 4.1: Gliding Crash Geometry ([1], Figure 2)

the aircraft reaches the average pedestrian height, injuries will occur within the area defined by its length and wingspan as it continues to glide to the ground. The relevant geometry is shown in Figure 4.1.

With this model, the number of injuries or fatalities expected from a crash is then found as

$$\text{Expected Injuries per Crash} = I_{crash} = \sigma_P \times (w_{UA} + 2R_P) \times \left(L_{UA} + \frac{H_P}{\tan\gamma} + 2R_P \right) \tag{4.1}$$

where σ_P is the pedestrian density, w_{UA}, L_{UA}, γ are the wingspan, length, and glide angle of the UAS respectively, and R_P and H_P are the average pedestrian radius and height. On a broad scale, then, we may obtain the expected number of injuries per flight hour by simply multiplying this by the average crash frequency, λ:

$$\text{Expected Injuries per Flight Hour} = I_{Flight\,Hour} = \lambda \times \sigma_P \times (w_{UA} + 2R_P) \times (L_{UA} + \frac{H_P}{\tan\gamma} + 2R_P) \tag{4.2}$$

4.1.2 Model Validation and Comments

Validation of the "gliding crash" model is an important concern; a simple model is not useful if it does not make reasonably accurate predictions. Since both manned and unmanned will incur similar bystander injuries in the event of a crash, historical manned crash data documented by the NTSB provides a useful benchmark for this purpose. While several parameters vary in the model, some simplifying assumptions are made in the following analysis. First, while glide angle does vary between different aircraft, its effect between different manned aircraft on the predicted injuries is minimal and thus a constant glide angle of 2.5 degrees is used below. Secondly, since the length of the aircraft scales roughly with its wingspan, we take $L_A \approx w_A$ in our analysis. Next, the aircraft failure rate is assumed to be the historical class A mishap rate of 15.3 failures per 100,000 flight hours. Finally, while perhaps 10% of the population is outside (and thus vulnerable) at any given time, in order to account for all injuries as opposed to just fatalities (which may result from flying debris, fires started, and the lack of protection offered by buildings due to impact by large aircraft, etc.), we shall assume that the pedestrian density is equal to the population density. A summary of these assumptions and parameter values used is found in Table 4.1. With these assumptions in place, the effects of two important variables remain to be considered: aircraft wingspan, w_A, and population density, σ_P. Both floating histograms (described in Section 2) and cumulative probability distributions are used to compare the model-estimated hazard rates to historical rates while controlling for these parameters.

Figure 4.2 uses a floating histogram as one of the comparisons. The left-hand side of the figure shows ground injuries versus population density, where aircraft size is controlled for by scaling injuries to a one meter wingspan aircraft. The right-hand side plots average ground injuries vs wingspan, where the model estimate uses the average population density of the locations in which crashes occurred in order to control for

Parameter	Value
H_p	1.75 m
R_p	0.25 m
γ	2.5 deg
L_A	w_A
σ_p	$\sigma_{population}$
λ	1.53×10^{-4} failures per flight hour

Table 4.1: Ground Collision Model Parameters

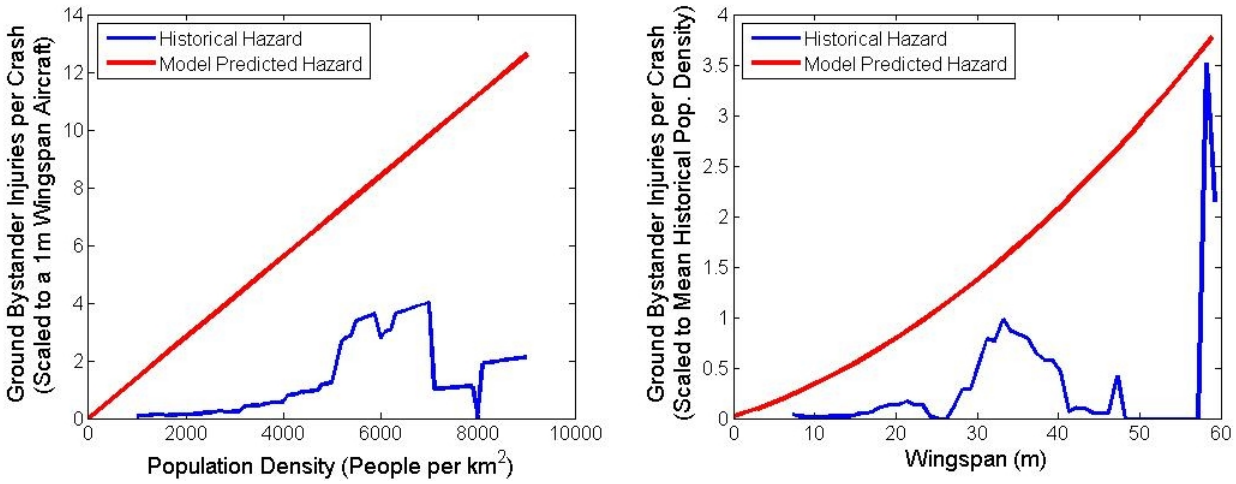

Figure 4.2: Floating Histogram Comparison of Historical and Model-estimated Risk for the Entire US

this variable. In both of these cases, the model predicts the ground bystander injuries to first order. Since it provides a conservative estimate of the average number of injuries when a crash occurs in a given location, this is acceptable.

Figure 4.3 uses a cumulative probability distribution as a comparison between historical hazard and model estimates. The cumulative probability distribution comparison plots for each X the likelihood given that an injury occurred, that it occurred at a value less than or equal to X. We consider this distribution versus population density on the left side of the figure and versus wingspan on the right side. For the distribution plotted versus population, we see that the historical and model predicted probability distributions match fairly well for low population density levels but deviate at high levels. With the relative dearth of data for higher population densities, this tells us that the model correctly incorporates population density as a linear factor in injuries. On the other hand, the distribution plotted versus wingspan shows reasonable correspondence between historical hazard and that predicted by the model only for very low wingspans, then deviates sharply. However, upon comparison with the floating histogram data, we note that the lack injury data for wingspans between approximately 45 and 55 meters naturally skews the historical distribution upwards below this point. For instance, Figure 4.4 shows how the distributions would compare if a low but non-zero value of 0.1 average injuries is inserted into the historical data set in this range. While this is by no means a definitive demonstration, combined with the floating histogram data it does show that the model likely correctly incorporates wingspan data.

We have shown that the "gliding crash" model accurately incorporates the effects of population density and wingspan on bystander injuries. It furthermore provides a first-order conservative estimate of the bystander injuries given a crash by a particular aircraft in a known location. This model gives us an important insight for analyzing UAS missions: for any particular UAS, the surface-level bystander harm rate is a function only of population density.

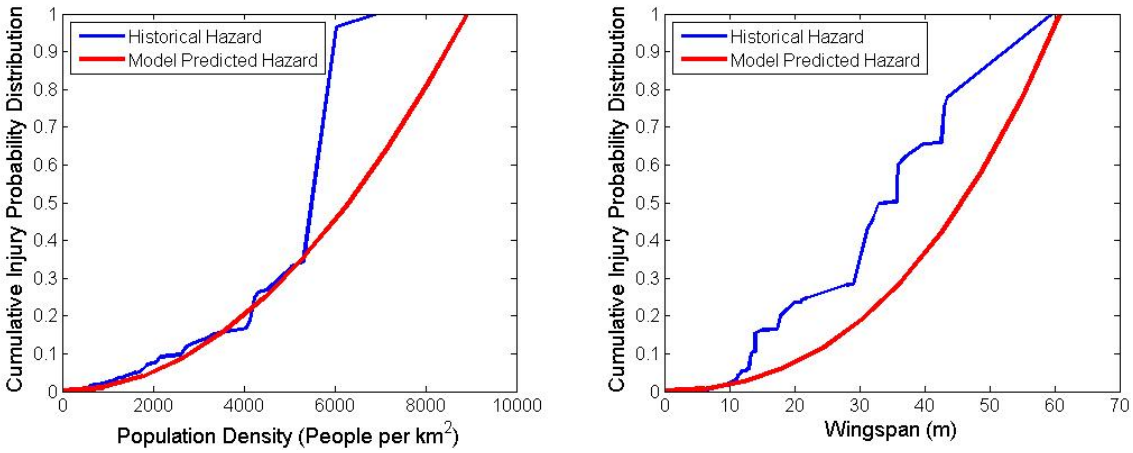

Figure 4.3: Cumulative Injury Probability Distributions of Historical and Model-estimated Risk for the Entire US

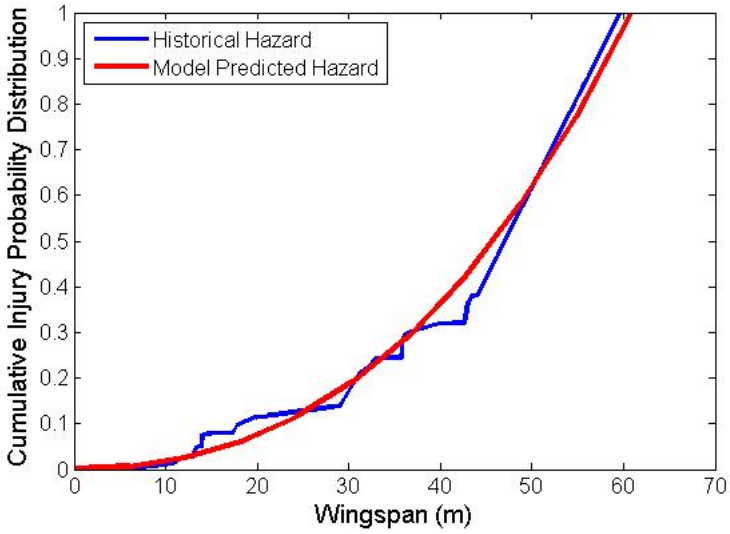

Figure 4.4: Cumulative Injury Probability Distributions for the Entire US with fake Historical Data Added Between 45 and 55 m.

4.2 Likelihood of a Crash

4.2.1 Aircraft Failure Rate near Airports

When and where do we expect a crash-inducing failure to occur? We often hear statistics such as "Aircraft x has y failures per ten-thousand flight hours," which assumes that a crash could occur in any location and at any time with equal probability. While this is a useful assumption on a broad scale (as in Equation 4.2), equal probability of failure is not accurate near an airport during which time an aircraft is either taking off or landing. If an aircraft is not airworthy, for instance a serious engine problem exists, a resultant crash is more likely to occur closer to the airport. Other potential problems such as vulnerability to weather, flocks of birds, etc. can be linked to lower altitudes and thus to the distance from the airport as well.

In fact, the crash rate per aircraft-hour increases greatly near airports, as is shown in Figure 4.5. Here, the cumulative number of historic crashes (per movement) of aircraft at Chicago O'Hare, JFK, and Miami International airports are plotted versus distance from the airport. If we define $P(r)$ to be the crashes per movement as a function of distance to the airport, then this figure plots its integral,

$$\int_0^d P(r)dr \tag{4.3}$$

We see the variability of $P(r)$ as the initially rapid accumulation of crashes tapers off as the distance from the airport grows. By the thirty kilometer mark, very few additional crashes occur.

It should be noted that these effects, as well as the resulting injuries to bystanders, are independent of aircraft density near the airport. While aircraft density does increase near an airport, the flux of aircraft (and thus total flight hours) through any perimeter is constant, as shown in Figure 4.6. This means that the total number of crashes (barring mid-air collisions) at a given distance is due to operational issues, not geometric ones. The effects of aircraft density are explored in Section 4.3.

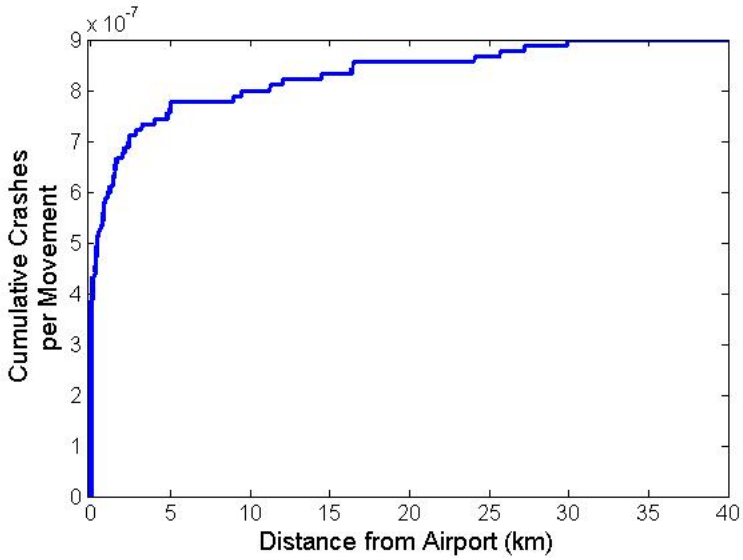

Figure 4.5: Cumulative Crash Distribution, per Movement, near Chicago O'Hare, JFK, and Miami International Airports

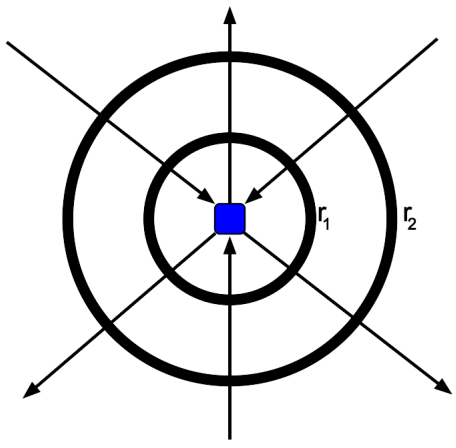

Figure 4.6: Aircraft Flux is Constant through Different Radial Boundaries

4.2.2 Total Injuries near Airports

Previously, we investigated the ability of the "gliding crash" model to predict bystander injuries given a crash, which was validated with data from across the US. However, the question that arises is if this model remains valid in the local-airport domain, or if it only applies to the continental-scale area? If the crash-inducing failures per movement as a function of distance is $P(d)$, then the total number of injuries near an airport as a function of distance, $I_{Airport\,per\,Movement}(d)$, is predicted to be

$$I_{Airport\,per\,Movement}(d) = P(d) \times I_{crash} \tag{4.4}$$

where I_{crash} is once again the expected number of injuries per crash from our general hazard estimation model. This formula is simply a combination of the "gliding crash" model (for how many injuries are expected per crash) and the local failure distribution (for where these crashes are likely to occur).

Using the cumulative crashes per movement distribution from Section 4.2.1, we may then use the model-predicted injury function to compare the predicted and actual injuries per movement. Figure 4.7 does this by plotting the cumulative injury distribution

$$I_{Cum.\,per\,Movement}(d) = \int_0^d I_{Airport\,per\,Movement}(r)\,dr \tag{4.5}$$

near the airports. Here, the model estimation used the aircraft-movement-weighted mean of the three cities' population densities as the population density input, and the average wingspan of the historical accidents for the aircraft wingspan input. The cumulative historical injuries were plotted without scaling other than dividing by total movements over the sample period. Our model provides a good, conservative bounding of the actual injuries; the only place where this is unclear is at very small distances (less than 1 km). In fact, however, the model correctly bounds the injuries here as well, with no injuries historically occurring on the edge of the airports' boundaries in our data set. The model serves as a good predictor of the total bystander risk near

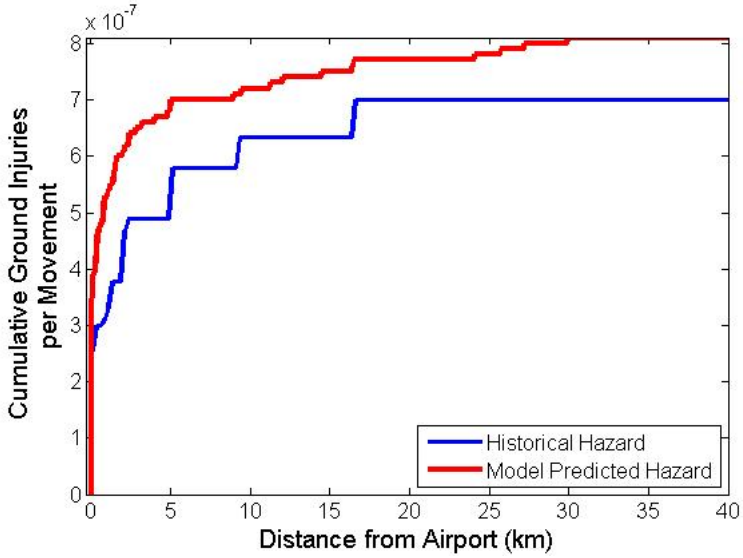

Figure 4.7: Historical versus Model-estimated Cumulative Injury Distributions, per Movement

an airport, as injuries occur as predicted by the general hazard model when the local, non-constant crash distribution is taken into consideration. These results also give some insight into planning UAS missions. They imply that we must be careful in our choice of airports for these missions, as the risk for injuring surface-level bystanders is high in the immediately surrounding area.

4.3 Bystander Perspective Hazard

Let us now consider the hazard rate from the perspective of a bystander near an airport. Unlike the total injury case near airports discussed above, from the bystander's perspective the density of aircraft *does* matter. This is due to the fact that, while the total number of injuries is related to the total flux of aircraft at a given radius from the airport (and thus related to total movements since this flux is conserved at different distances), a bystander is worried about whether a crash will injure them specifically. Consider a bystander who occupies a fixed area dA on an annulus of radius r and

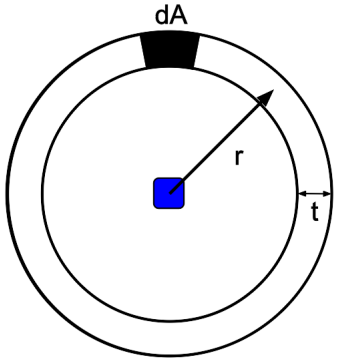

Figure 4.8: Plane Density near an Airport

constant thickness t, centered on the airport as in Figure 4.8. As the radius of the annulus increases, the total number of aircraft in this airspace, N, remains constant as has been mentioned previously. However, we see that the *density* of aircraft as a function of radius, $\rho(r)$, is

$$\rho(r) = \frac{N}{\pi\left(\left(r+\frac{t}{2}\right)^2 - \left(r-\frac{t}{2}\right)^2\right)} \tag{4.6}$$

or equivalently,

$$\rho = \frac{N}{2\pi r t} \tag{4.7}$$

varies with the inverse of radius. Given that a crash occurs at a certain radius, a bystander is less likely to get hit as the distance from the airport is increased since the crash is equally likely to occur anywhere in the annulus. The total injuries will remain constant, but the average injuries per unit area will decrease.

We may combine this information with the historical, airport-local injury distributions found above to calculate the hazard rate from the bystander's perspective. Looking at the effective radius of the airports used to collect the historical data, we find that $r_{min} = 1.25\,\text{km}$ is a representative radius for the airport boundary; this is

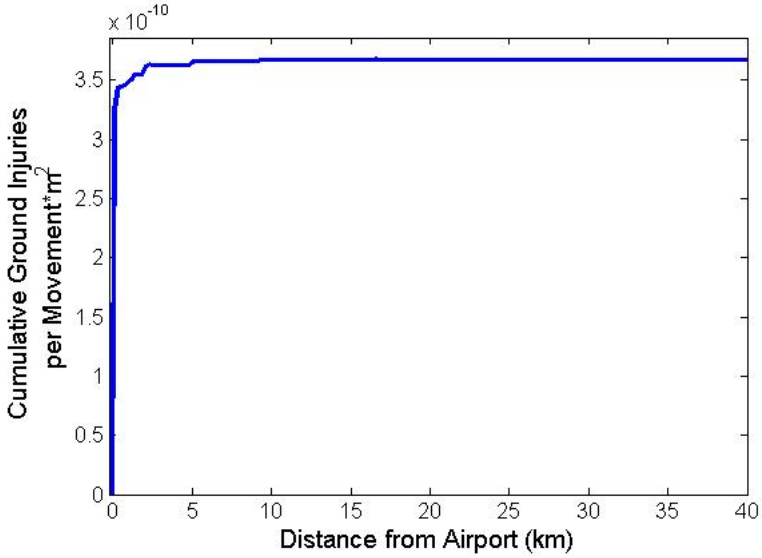

Figure 4.9: Cumulative Injuries Density near an Airport

also approximately half the necessary runway length for medium-sized aircraft. This can then be used as the starting radius for our annulus (corresponding to zero distance from the airport in our plots). The injury density per movement, $I_{Density\,per\,Movement}$, is then calculated as

$$I_{Density\,per\,Movement}(d) = \frac{I_{Airport\,per\,Movement}(d)}{2\pi(d + r_{min})t} \tag{4.8}$$

and the cumulative injury density per movement, $I_{Cum.\,Density\,per\,Movement}(d)$, is calculated as

$$I_{Cum.\,Density\,per\,Movement}(d) = \int_0^d \frac{I_{Cum.\,per\,Movement}(r)}{2\pi(r + r_{min})t}\,dr \tag{4.9}$$

Taking a characteristic thickness of $t = 1\,\text{m}$, the historical cumulative injuries density per movement meter squared are plotted in Figure 4.9. As compared to the cumulative injuries per movement, Figure 4.7, we see that the cumulative injury density levels out extremely quickly, even though injuries still occurring at larger distances.

If, as above, we say that bystanders have characteristic radius $R_p = 0.25\,\text{m}$, we may furthermore calculate the bystander perspective injuries per movement, $I_{Bystander\,per\,Movement}$,

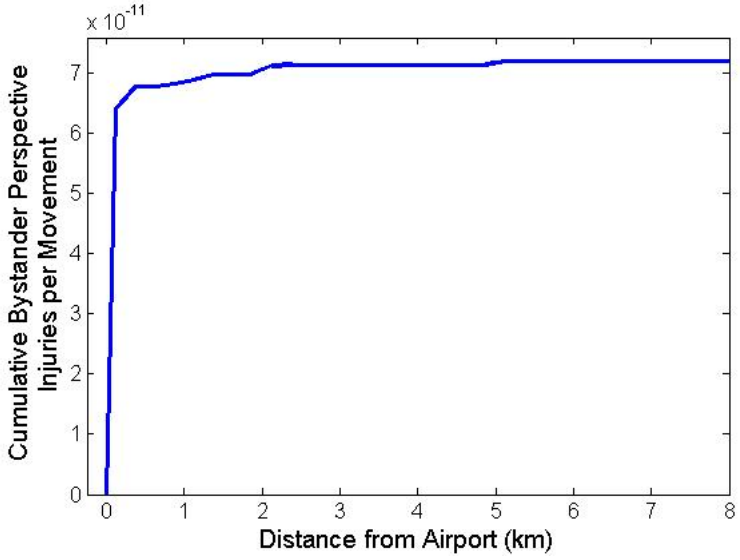

Figure 4.10: Cumulative Bystander Perspective Hazard near an Airport

as

$$I_{Bystander\,per\,Movement} = I_{Density\,per\,Movement}(d) \times \pi R_p^2 \tag{4.10}$$

and the cumulative bystander perspective injuries per movement, $I_{Cum.\,Bystander\,per\,Movement}$, as

$$I_{Cum.\,Bystander\,per\,Movement} = I_{Cum.\,Density\,per\,Movement}(d) \times \pi R_p^2 \tag{4.11}$$

the latter of which is shown in Figure 4.10. This figure clearly shows how, from the bystander's perspective, the combination of the decreased failure rate and the decreased aircraft density very rapidly diminishes the hazard rate as the distance from the airport is increased.

Chapter 5
EXAMPLE RISK ASSESSMENT

This chapter presents examples of using the methedology of this research for assessing the risk of UAS missions in various environments. The first example presents general results across the continental United States, while the second example provides a more detailed look at a particular proposed mission profile.

5.1 Risk of Flying in US Counties

As UAS are integrated into the national airspace, the question of where they can be safely flown naturally occurs. For example, if a proposed mission is for a UAS to patrol a national forest searching for signs of forest fires, a quick reference is desired of the risk to bystanders in this area. As a demonstration of the simplicity of the ground collision model investigated in Section 4.1, maps detailing the injury rate per crash across the United States have therefore been developed.

	ScanEagle	**MQ-9 Reaper**	**Boeing 737**
w_{UA}	3 m	10 m	28.9 m
L_{UA}	1.5 m	11 m	35 m
γ	3.18 deg	2.3 deg	3.75 deg

Table 5.1: UAS Characteristics

Using Equation 4.1, the hazard rate per crash was calculated in each county in the continental Unites States. Figure 5.1 shows the risk to bystanders per crash of a Scangeagle-sized aircraft across the United States, while Figure 5.2 shows the risk per

crash of an MQ-9-sized aircraft, and Figure 5.3 does the same for a 737-sized aircraft. Characteristics of these aircraft may be found in Table 5.1. The cooler areas in both of these maps correspond to lower risk, while hotter colors correspond to higher risk. The colors associate directly with the population density in each county. For example, Los Angeles County in California has a very high population density and therefore a high risk of injury to bystanders from an aircraft crash. However, large swathes of the country have much, much lower population density than this, and therefore represent much safer areas for UAS operation.

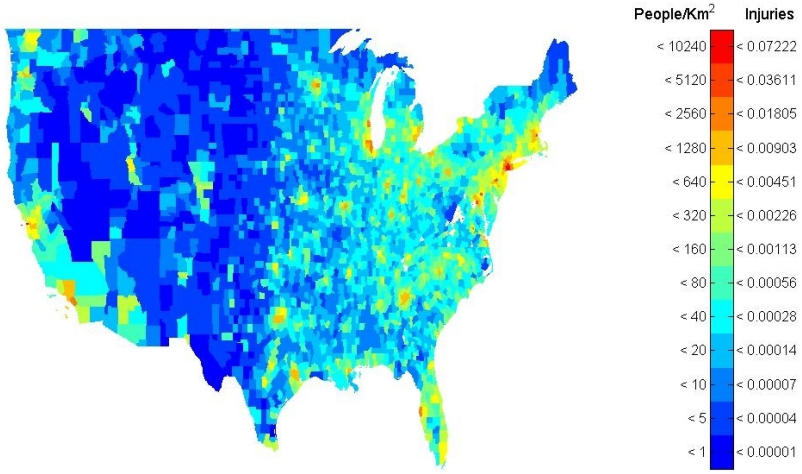

Figure 5.1: Estimated Injuries Given a Crash by a ScanEagle-sized Aircraft

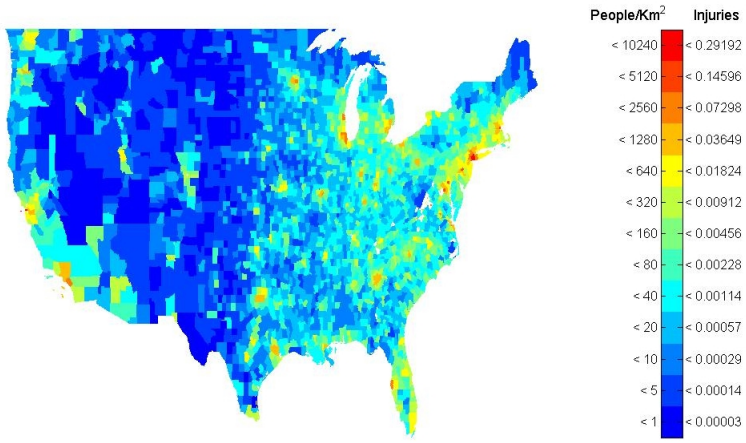

Figure 5.2: Estimated Injuries Given a Crash by an MQ-9-sized Aircraft

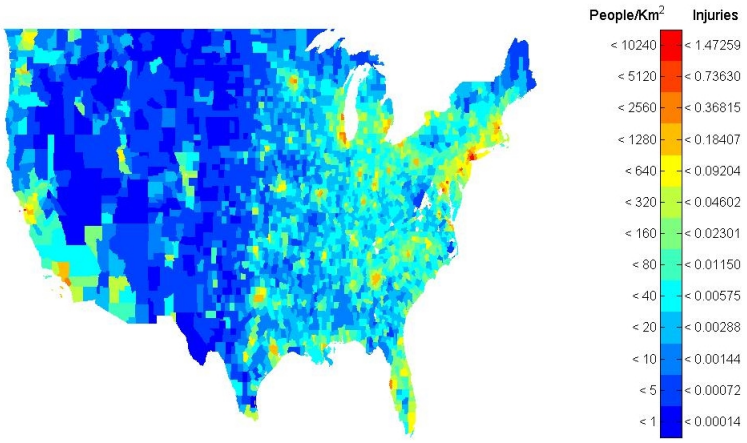

Figure 5.3: Estimated Injuries Given a Crash by a 737-sized Aircraft

5.2 UAS Test Range

Following the FAA Modernization and Reform Act of 2012, the FAA began a search for viable UAS test sites [2]. These sites are intended to provide information that will aid the safe integration of UAS into the national airspace, and will influence new FAA policies and procedures regulating their use. One such proposed test site is located in Moses Lake, Washington.

	MQ-9 Reaper	**ScanEagle**
w_{UA}	10 m	3 m
L_{UA}	11 m	1.5 m
γ	2.3 deg	3.18 deg
λ_{UA}	1.5×10^{-4} failures per flight hour	1×10^{-3} failures per flight hour

Table 5.2: UAS Characteristics

As part of the proposal, two UAS air corridors were presented. A primary corridor links Moses Lake to Greys Harbor, while an alternate corridor would link the test range to the Dalles Airport. A risk analysis was performed for UAS operations in the Moses Lake range, as well as along the corridors, in order to help show the feasibility of this proposed test site. Since test sites such as the proposed Moses Lake site will be utilized by UAS of many different sizes and with different reliability rates, the analysis was carried out for both an MQ-9 Reaper as well as a ScanEagle in order to represent this wide range of possibilities. Characteristics of these two vehicles can be found in Table 5.2.

Figure 5.4 shows the region of interest. In this map, the red circles represent various cities in the area, with circle size proportional to population density. The blue dotted lines represent the legs of the proposed path linking Moses Lake, in the East, to Greys Harbor, in the West. Similarly, the magenta lines mark the alternate

leg linking Moses Lake to the Dalles Airport. These paths were picked to avoid densely populated areas while also skirting the major manned aircraft corridors in the region.

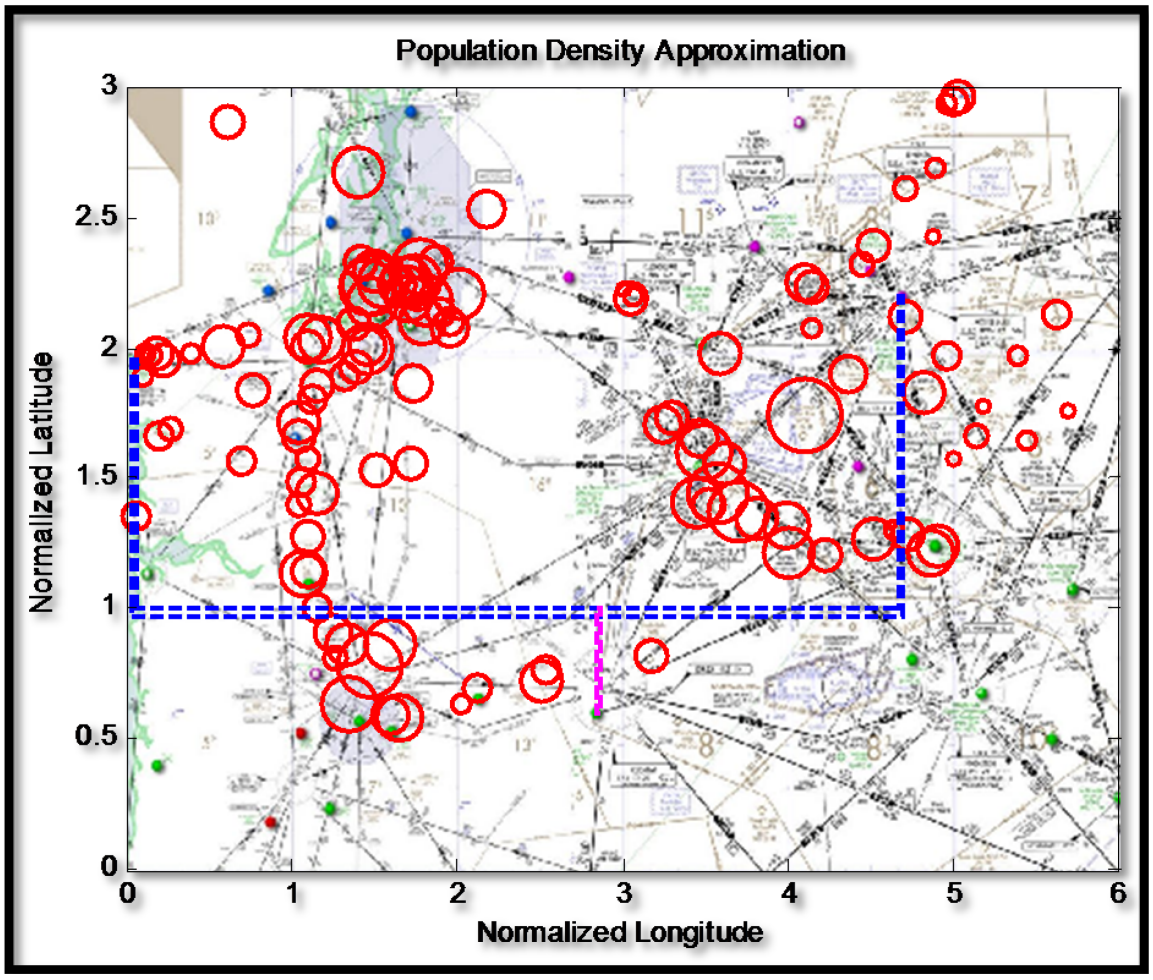

Figure 5.4: Corridor Assessment Between Greys Harbor, Moses Lake, and Dalles Airport

Table 5.3 lists the relevant population density and length of each leg of the various paths. The expected injuries per flight hour for each leg as well as within the Moses Lake Test Range were calculated using Equation 4.2, and can be found on the right side of this table. The model predictions for each leg were then combined using

a path-leg-length weighted average to find the overall values for the two paths, as presented in Table 5.4. This table also includes the expected cumulative injuries near the airport, calculated using Equations 4.4 and 4.5 and the historical, manned crashes per movement data of Figure 4.5. From these results, it is clear that for many types of UAS it would be safe to fly along the proposed corridors to and from Moses Lake as necessary. Further, extended operations within the Moses Lake test site would be safe for surface-level bystanders in the region, with more than one hundred million aircraft movements per expected bystander injury for either the MQ-9 Reaper or the ScanEagle.

Flight Leg	**Population Density** $\left[\text{People} \cdot \text{km}^{-2}\right]$	**Leg Length** [km]	**Injuries per Flight Hour**	
			MQ-9 Reaper	**ScanEagle**
Leg 1 – South from Moses Lake	520	120	8.97×10^{-5}	6.09×10^{-5}
Leg 2 – West towards the coast	327	370	5.64×10^{-5}	3.83×10^{-5}
Leg 3 – North to Greys Harbor	398.	93	6.88×10^{-5}	4.67×10^{-5}
Leg 4 – West towards Dalles	327	144	5.64×10^{-5}	3.83×10^{-5}
Leg 5 – South towards Dalles	828	44	1.43×10^{-4}	9.71×10^{-5}
Within Moses Lake Test Range	2.7	N/A	4.7×10^{-7}	3.2×10^{-7}

Table 5.3: UAS Flight Leg Data

	Flight Path	**Injuries**	
		MQ-9 Reaper	**ScanEagle**
	Moses Lake to Greys Harbor	6.52×10^{-5} [Flight Hour^{-1}]	4.43×10^{-5} [Flight Hour^{-1}]
	Moses Lake to Dalles	8.18×10^{-5} [Flight Hour^{-1}]	5.55×10^{-5} [Flight Hour^{-1}]
Within Moses Lake Test Range	Cumulative Injuries, 5 miles from runway	9.1×10^{-9} $\left[\text{Movement}^{-1}\right]$	6.2×10^{-9} $\left[\text{Movement}^{-1}\right]$
	Cumulative Injuries, 10 miles from runway	9.9×10^{-9} $\left[\text{Movement}^{-1}\right]$	6.6×10^{-9} $\left[\text{Movement}^{-1}\right]$

Table 5.4: UAS Overall Flight Paths

Chapter 6

CONCLUSIONS

6.1 Summary of Results

Unmanned Aerial Systems provide a breadth of possibilities for use in the United States. However, we must cast a careful eye on the inherent hazards of operating these systems as they are integrated into the national airspace. In particular, mission feasibility must include an analysis of the risk to human bystanders.

By analysis of historical manned data as compared to the random particle collision rate, Section 3 showed that general aviation aircraft flying under visual flight rules routinely operate in conditions where see-and-avoid is not effective. Therefore, while sense-and-avoid capabilities will only decrease the risk of midair collisions, UAS already achieve equivalent manned levels of safety in this area. It is clear that, despite public perception, midair collisions between UAS and manned aircraft are not the primary source of hazard in the national airspace.

Concerning the hazard to surface-level bystanders from ground collisions, we showed in Section 4 that a simple model was sufficient to provide a first-order, conservative estimate of the risk. This was done once again by comparing the model estimates to historical aircraft accident data. Through this analysis, we showed that, on a broad scale, population density is the discriminating factor when assessing mission feasibility for a particular UAS. On a local level, however, the factor of distance from the operating airport becomes important; this is because crash rates are much higher near airports. The ground collision hazard model was then verified for this near-airport risk as well, taking into account the variations in crash rate there. Finally, the bystander perspective risk was considered. We showed that from this vantage

point, aircraft density matters greatly as it influences the likelihood of a particular bystander getting harmed in a given region. Therefore, as distance to an airport increases, the bystander perspective risk drastically drops due to the combination of decreasing crash rates and decreasing aircraft density.

Applying these insights, Section 5 presented how a simple risk analysis can be applied to proposed UAS missions. For the continental United States, we showed how the ground collision risk varies on a broad scale from county to county. This demonstrated the direct link between population density and the risk to human bystanders. We then turned our attention towards a proposed UAS test range iat Moses Lake, Washington. While the test site itself is located in a sparsely populated area, two potential air corridors necessarily cross over inhabited regions. Though they consist of multi-leg paths in order to skirt around the densest population centers, we showed how to analyze the risk of flying through these corridors as well as of operating solely in the proposed test range.

The insights and simple tools demonstrated here are important as they be used to help analyze and plan proposed UAS missions, both from a high level as well as a detail oriented perspective. They are also important, however, because they show that UAS can be safely operated over the majority of the United States.

6.2 Future Work

One possible extension to this work would involve subdividing historical midair collisions by altitude and distance from the operating airports. This would allow us to address the lack of homogeneity in manned aircraft flights around the country. For instance, we would expect a higher incidence of collisions near airports due to higher aircraft density there. Analysis of this sort could give further insight into the causes of midair collisions, as well as where policy improvements and possible technological upgrades may need to be made.

Another possibility is adapting the random particle model to better model the

interaction between managed air carrier traffic and general aviation traffic. Air carriers usually fly through "highways in the sky," air corridors with traffic in only one direction and fairly uniform airspeed. When these highways interact with the more random general aviation traffic, the random motion assumed in the derivation of the random particle collision model changes. It would be instructive to see how well the historic accidents between air carriers and general aviation match with such an adapted model.

In the domain of ground collisions, more work remains in analyzing crash likelihood. In particular, it would be instructive to gather more data in various locations on the distances between accidents and the aircraft's operating airport. This would allow us to make stronger and more general statements about near-airport risk. Furthermore, additional information on characteristic crash locations and any differences in this regard between UAS and manned aircraft crashed could provide significant insights when analyzing the risk of UAS missions.

BIBLIOGRAPHY

[1] C. W. Lum and B. Waggoner, "A risk based paradigm and model for unmanned aerial systems in the national airspace," in *AIAA Infotech@Aerospace Conference*, March 2011.

[2] FAA, `http://www.faa.gov/about/initiatives/uas/`, *Programs & Initiatives: Unmanned Aircraft Systems (UAS)*. Online; accessed 01-July-2013.

[3] R. E. Weibel and R. J. Hansman Jr, "An integrated approach to evaluating risk mitigation measures for uav operational concepts in the nas," *Proceedings of InfoTech at Aerospace: Advancing Contemporary Aerospace Technologies and Their Integration*, vol. 1, pp. 509–519, 2005.

[4] R. E. Weibel and R. J. Hansman, "Safety considerations for operation of unmanned aerial vehicles in the national airspace system," 2006.

[5] H. P. Shuch, "General aviation collision-avoidance alternatives," *Journal of Transportation Engineering*, vol. 115, no. 5, pp. 474–492, 1989.

[6] M. J. Kochenderfer, M. W. Edwards, L. P. Espindle, J. K. Kuchar, and J. D. Griffith, "Airspace encounter models for estimating collision risk," *Journal of Guidance, Control, and Dynamics*, vol. 33, no. 2, pp. 487–499, 2010.

[7] H.-T. Lee, L. A. Meyn, and S. Kim, "Probabilistic safety assessment of unmanned aerial system operations," *Journal of Guidance, Control, and Dynamics*, vol. 36, no. 2, pp. 610–617, 2013.

[8] J. Asmat, B. Rhodes, J. Umansky, C. Villavicencio, A. Yunas, G. Donohue, and A. Lacher, "Uas safety: Unmanned aerial collision avoidance system (ucas)," in

2006 IEEE Systems and Information Engineering Design Symposium, pp. 43–49, IEEE, 2006.

[9] N. L. Fulton, M. Westcott, and S. Emery, "Decision support for risk assessment of mid-air collisions via population-based measures," *Transportation Research Part A: Policy and Practice*, vol. 43, no. 2, pp. 150–169, 2009.

[10] K. Dalamagkidis, K. P. Valavanis, and L. A. Piegl, "Evaluating the risk of unmanned aircraft ground impacts," in *2008 16th Mediterranean Conference on Control and Automation*, pp. 709–716, IEEE, 2008.

[11] C. W. Lum, K. Gauksheim, T. Kosel, and T. McGeer, "Assessing and estimating risk of operating unmanned aerial systems in populated areas," in *11th AIAA Aviation Techonology, Integration, and Operations (ATIO) Conference*, 2011.

[12] R. A. Clothier, R. A. Walker, N. Fulton, and D. A. Campbell, "A casualty risk analysis for unmanned aerial system (uas) operations over inhabited areas," in *Twelfth Australian International Aerospace Congress*, 2007.

[13] P. P. Wu and R. A. Clothier, "The development of ground impact models for the analysis of the risks associated with unmanned aircraft operations over inhabited areas," in *Proceedings of the 11th Probabilistic Safety Assessment and Management Conference (PSAM11) and the Annual European Safety and Reliability Conference (ESREL 2012)*, 2012.

[14] F. Netjasov and M. Janic, "A review of research on risk and safety modelling in civil aviation," *Journal of Air Transport Management*, vol. 14, no. 4, pp. 213–220, 2008.

[15] NTSB, `http://www.ntsb.gov/avdata/`, *Aviation Accident Database*. Online; accessed 15-March-2012.

[16] U.S. Census Bureau, http://factfinder2.census.gov/faces/nav/jsf/pages/index.xhtml, *Census 2010 Summary File 1.* Online; accessed 02-May-2012.

[17] NTSB, http://www.ntsb.gov/investigations/reports_aviation.html, *Aviation Accident Reports.* Online; accessed August-2012.

[18] Embry-Riddle Aeronautical University, http://prcarc1.erau.edu/index.html, *Aviation Safety and Security Archives.* Online; accessed 28-August-2012.

[19] FAA, http://www.faa.gov/data_research/aviation_data_statistics/general_aviation/, *General Aviation and Part 135 Activity Surveys.* Online; accessed August-2012.

[20] J. Anno, "Estimate of human control over mid-air collisions," *Journal of Aircraft*, vol. 19, no. 1, pp. 86–88, 1982.